



Nitrogen oxides in the global upper troposphere: interpreting cloud-sliced NO_2 observations from the OMI satellite instrument

Eloise A. Marais^{1,2}, Daniel J. Jacob^{2,3}, Sungyeon Choi⁴, Joanna Joiner^{4,5}, Maria Belmonte-Rivas⁶, Ronald C. Cohen^{7,8}, Steffen Beirle⁹, Lee T. Murray¹⁰, Luke Schiferl^{11,*}, Viral Shah¹², Lyatt Jaeglé¹²

5 ¹School of Geography, Earth, and Environmental Sciences, University of Birmingham, Birmingham, UK.

²John A Paulson School of Engineering and Applied Sciences, Harvard University, Cambridge, MA, USA.

³Earth and Planetary Sciences, Harvard University, Cambridge, MA, USA.

⁴Science Systems and Applications Inc., Lanham, MD.

⁵NASA Goddard Space Flight Center, Greenbelt, MD.

10 ⁶Royal Netherlands Meteorology Institute, De Bilt, the Netherlands.

⁷Department of Chemistry, University of California at Berkeley, Berkeley, CA.

⁸Department of Earth and Planetary Science, University of California at Berkeley, Berkeley, CA.

⁹Max-Planck-Institut für Chemie, Mainz, Germany.

¹⁰Department of Earth and Environmental Sciences, University of Rochester, Rochester, New York, USA.

15 ¹¹Department of Civil and Environmental Engineering, Massachusetts Institute of Technology, Cambridge, USA.

¹²Department of Atmospheric Sciences, University of Washington, Seattle, WA, USA.

* Now at: John A Paulson School of Engineering and Applied Sciences, Harvard University, Cambridge, MA, USA.

Correspondence to: Eloise A. Marais (e.a.marais@bham.ac.uk)

Abstract. Nitrogen oxides ($\text{NO}_x \equiv \text{NO} + \text{NO}_2$) in the upper troposphere (UT) have a large impact on global tropospheric ozone and OH (the main atmospheric oxidant). New cloud-sliced observations of UT NO_2 at 450-280 hPa (~6-9 km) from the OMI satellite instrument produced by NASA and KNMI provide global coverage to test our understanding of the factors controlling UT NO_x . We find that these products offer useful information when averaged over coarse scales ($20^\circ \times 32^\circ$, seasonal), and that the NASA product is more consistent with aircraft observations of UT NO_2 . Correlation with LIS/OTD satellite observations of lightning flash frequencies shows that lightning is the dominant source of NO_x to the upper troposphere except for extratropical latitudes in winter. We infer a global mean NO_x yield of 280 moles per lightning flash, with no significant difference between the tropics and mid-latitudes, and a global lightning NO_x source of 5.6 Tg N a⁻¹. There is indication that the NO_x yield per flash increases with lightning flash footprint and with flash energy.

20
25

1. Introduction

Nitrogen oxides ($\text{NO}_x \equiv \text{NO} + \text{NO}_2$) in the upper troposphere (UT) have profound effects on the oxidizing capacity of the atmosphere and on climate, but the factors controlling their concentrations are poorly understood. Here we use two new satellite products of UT NO_2 mixing ratios from the Ozone Monitoring Instrument (OMI), together with in situ aircraft measurements and the GEOS-Chem chemical transport model, to assess current understanding of UT NO_x sources.

30

NO_x in the UT impacts climate by efficiently producing ozone where it is a potent greenhouse gas (Dahlmann et al., 2011; Worden et al., 2011; Rap et al., 2015) and by increasing the concentration of OH (the main tropospheric oxidant) (Murray et al., 2012; 2014). Primary NO_x sources in the UT include lightning, aircraft, convective injection, and downwelling from the stratosphere (Ehhalt et al., 1992; Jaeglé et al., 1998b; Bertram et al., 2007). NO_x cycles chemically with reservoir species including nitric acid (HNO_3), pernitric acid (HNO_4), dinitrogen pentoxide (N_2O_5), peroxyacetyl nitrate (PAN), and other organic

35



40 nitrates, thus defining the NO_y chemical family ($\text{NO}_y \equiv \text{NO}_x + \text{reservoirs}$). Effective loss of NO_x from the UT is through subsidence of NO_y to lower altitudes where deposition of HNO_3 provides the ultimate sink. The residence time of NO_y in the UT is 10-20 days (Prather and Jacob, 1997). The lifetime of NO_x against conversion to short-lived reservoirs varies from ~3 hours in the convective outflow of thunderstorms to 0.5-1.5 days further afield (Nault et al., 2016). Chemical recycling from these reservoirs maintains relatively high UT NO_x background concentrations (Bradshaw et al., 2000; Baehr et al., 2003; Nault et al., 2016).

45

Representation of lightning NO_x in chemical transport models (CTMs) is highly uncertain. Physically-based parameterizations relating lightning frequency to deep convective cloud tops, convective mass flux, convective precipitation, or high-cloud ice content have poor predictive capability (Tost et al., 2007; Murray et al., 2012; Finney et al., 2014), limiting our ability to estimate the response of lightning NO_x to future climate (Finney et al., 2016; 2018). An alternative is to prescribe flash densities from space-based observations and static NO_x production rates per flash (Sauvage et al., 2007; Allen et al., 2010; Murray et al., 2012). NO_x production efficiencies per flash in the literature vary from <10 to 5000 moles nitrogen per flash (mol N ft^{-1}) (Schumann and Huntrieser, 2007; Murray, 2016). Global models typically use 100-500 mol N ft^{-1} , and a global lightning NO_x source of 3-7 Tg N a^{-1} , to match observations of tropospheric ozone and NO_y species (Denman and Brasseur, 2007).

55 Our understanding of UT NO_x has evolved mainly on the basis of observations from aircraft campaigns (Drummond et al., 1988; Jacob et al., 1996; Crawford et al., 1997; Jaeglé et al., 1998a; Bradshaw et al., 2000; Hudman et al., 2007; Stratmann et al., 2016). There are also long-term NO_x measurements from instruments onboard commercial aircraft dating back to the 1990s, but these are mostly over the north Atlantic and the NO_2 measurements have low precision and interference from thermally unstable NO_y reservoir compounds (Brunner et al., 2001).

60

Tropospheric column observations of NO_2 are obtained from space-based UV/visible spectrometers that measure solar-backscattered radiation. This provides global coverage, but with only one piece of vertical information. New cloud-sliced satellite NO_2 products at 280-450 hPa (~6-9 km) offer additional vertical resolution by retrieving partial NO_2 columns above clouds and exploiting differences in heights of neighboring clouds to calculate NO_2 mixing ratios (Belmonte-Rivas et al., 2015; Choi et al., 2014). A benefit of these satellite observations is continuous daily temporal and global spatial coverage. There are two new products of seasonal mean UT NO_2 mixing ratios retrieved from Ozone Monitoring Instrument (OMI) partial NO_2 columns by research groups at KNMI and NASA. The KNMI product has been evaluated against UT NO_2 from the Tracer Model version 4 (TM4) CTM. Large regional differences between OMI and TM4 are attributed to model deficiencies in lightning NO_x and uplift of anthropogenic pollution (Belmonte-Rivas et al., 2015). The NASA UT product is new to this work and follows a similar retrieval approach to the mid-tropospheric product of Choi et al. (2014). That product was evaluated with aircraft observations of NO_2 and interpreted with the Global Modeling Initiative (GMI) CTM (Choi et al., 2014). Dominant contributors to mid-troposphere NO_2 include pollution outflow, uplift of anthropogenic pollution, and lightning. Choi et al. (2014) identified large discrepancies between modeled and observed NO_2 seasonality over regions influenced by pollution and lightning.

75

Here we compare the two UT NO_2 products, obtained with distinct retrieval methods, and use aircraft observations of NO_2 from multiple NASA DC8 aircraft campaigns to arbitrate and evaluate the information that can be derived from the satellite datasets. We go on to test current understanding of UT NO_x using GEOS-Chem.



2. OMI observations of upper troposphere NO₂

80 OMI is onboard the NASA Aura satellite launched into sun-synchronous orbit in October 2004. It has an overpass time of about 13h30 local time (LT), a swath width of 2600 km, and a horizontal resolution of 13 km × 24 km at nadir (Levelt et al., 2006). Columns of NO₂ along the instrument viewing path (slant columns) are obtained by spectral fitting of solar backscattered radiation in the 405-465 nm window (Boersma et al., 2011). Standard products include total and tropospheric column NO₂ that are screened for cloudy scenes using a cloud radiance fraction threshold of 0.5. Partial columns of NO₂ above cloudy scenes can
85 be used to estimate vertically resolved NO₂ mixing ratios, as was first demonstrated with satellite observations of ozone (Ziemke et al., 2001). This approach, so-called cloud slicing, assumes a uniform trace gas concentration between two horizontally nearby clouds at different altitudes, so that the UT NO₂ mixing ratio is proportional to the slope of the partial columns versus the corresponding cloud pressures. Two UT NO₂ products have been retrieved from OMI: a product from KNMI at 330-450 hPa for 2006 (Belmonte-Rivas et al., 2015) and from NASA at 280-450 hPa for 2005-2007 following an approach similar to that used to
90 retrieve mid-tropospheric NO₂ (Choi et al., 2014). In what follows we distinguish the two OMI NO₂ products as KNMI and NASA.

The KNMI product uses DOMINO v2.0 slant columns (Boersma et al., 2011) and OMCLDO2 cloud fractions and altitudes (Acarreta et al., 2004) over partially to very cloudy scenes (cloud radiance fraction > 0.5). Contamination due to NO₂ from below
95 (up to 66% over polluted land masses) is estimated using the TM4 model and removed. Stratospheric NO₂ is from an assimilated product (Belmonte-Rivas et al., 2014) and is also removed. An air mass factor (AMF) that accounts for viewing geometry, surface albedo, light attenuation by gases and aerosols along the viewing path, and sensitivity to NO₂ vertical distribution is applied to the resultant UT slant columns to convert to vertical columns. Additional data filtering removes scenes with solar zenith angle (SZA) ≥ 70° and surface albedo ≥ 30%. Resultant daily vertical partial columns are aggregated on consistent
100 pressure and horizontal (1° × 1°) grids and used to determine seasonal mean UT NO₂ mixing ratios for gridsquares with at least 30 measurements. UT NO₂ at 330-450 hPa is estimated as the difference between columns at 380 hPa to the tropopause and at 380-500 hPa. Biases from sampling cloudy scenes, such as the effect of clouds on photochemistry, are corrected using TM4. These are small (typically <20%) in the upper troposphere (Belmonte-Rivas et al., 2015).

105 The NASA UT NO₂ product is for 2005-2007 at ~280-450 hPa and uses updated version 3 slant columns (OMNO2 v3.0) (Krotkov et al., 2017) that corrects for a positive bias in the DOMINO v2.0 product with improved spectral fitting (Marchenko et al., 2015; van Geffen et al., 2015). Partial columns are retrieved for individual OMI pixels above very cloudy scenes (cloud radiance fraction > 0.7) to minimize contamination from below. Cloud fraction and height is from the OMCLDO2 product (Acarreta et al., 2004). The AMF accounts for viewing path geometry and light scattering by near-Lambertian clouds. Data
110 filtering is applied to remove scenes with SZA > 80° and snow/ice cover and severe aerosol pollution that could be misclassified as clouds. Daily UT NO₂ is estimated for neighboring partial columns with sufficient cloud variability (cloud pressure distance > 160 hPa) and well-mixed NO₂ (NO₂ vertical gradient < 0.33 pptv hPa⁻¹ diagnosed with the GMI CTM). The stratospheric column is assumed uniform above neighboring clouds. Daily values of UT NO₂ are regridded to obtain seasonal means at 5° × 8° (latitude × longitude) for scenes with at least 50 measurements. Gaussian weighting is applied to assign higher weighting to UT
115 NO₂ closest to 350 hPa (Choi et al., 2014).

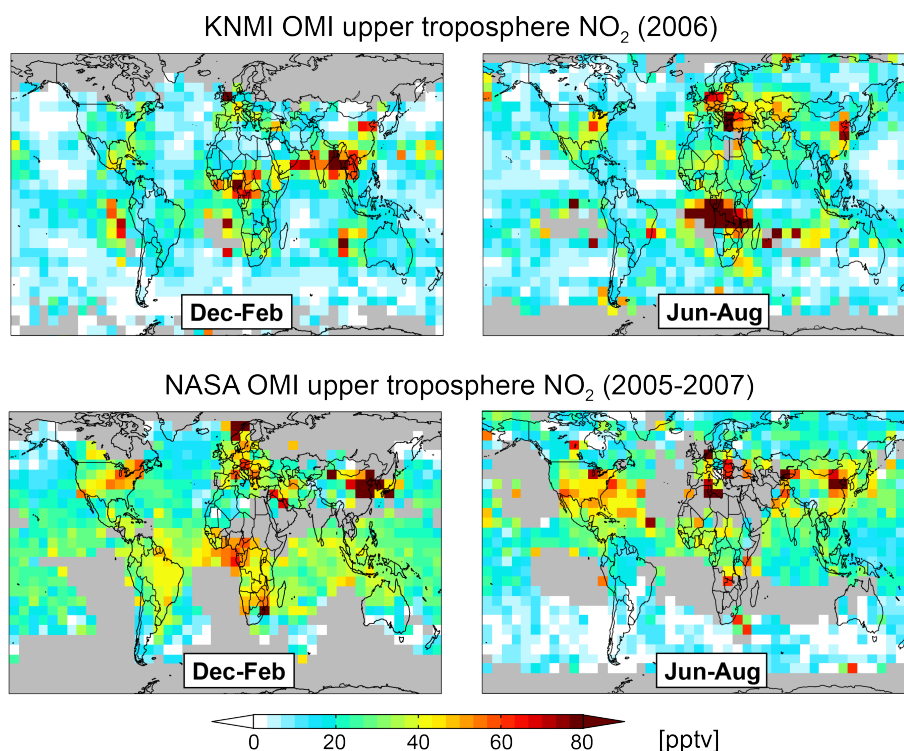
Figure 1 compares seasonal mean UT NO₂ from the two satellite products in December-February and June-August. KNMI NO₂ is regridded to the NASA coarse grid and NASA data are for 2005-2007. KNMI NO₂ has greater coverage than the NASA



product, due to a lower cloud fraction threshold in the retrieval. The two products exhibit very different spatial features.

120 Correlation between coincident gridsquares is weak ($R = 0.41$ in December-February, $R = 0.38$ in June-August). There is marginal improvement in the correlation with further spatial averaging. At $20^\circ \times 32^\circ$ $R = 0.50$ in December-February and $R = 0.45$ in June-August. The correlation only increases substantially in September-November from $R = 0.49$ at $5^\circ \times 8^\circ$ to $R = 0.66$ at $20^\circ \times 32^\circ$. KNMI is systematically lower than NASA in all seasons for coincident gridsquares, varying from 16% lower in June-August to 48% lower in December-February at $20^\circ \times 32^\circ$. The updated slant columns used by NASA correct for a high bias in

125 the operational product and so act in opposition to the discrepancies between the two products.



130 **Figure 1. Upper troposphere (UT) NO_2 from the OMI satellite instrument. Seasonal mean UT NO_2 from KNMI in 2006 at 330-450 hPa (top) is compared to NASA in 2005-2007 at 280-450 hPa (bottom). Data are at $5^\circ \times 8^\circ$ horizontal resolution for December-February (left) and June-August (right). Grey areas indicate no data and, for NASA, scenes with fewer than 50 measurements.**

Contamination of UT NO_2 from below and from convective uplift appears in both products, despite attempts to correct for this in the case of KNMI and avoid this by only considering very cloudy scenes in the case of NASA. These include a large enhancement in KNMI NO_2 (> 90 pptv) over southern Africa in June-August when there is intense biomass burning, and the

135 NO_2 hotspot over northeast China in all seasons in both products.

3. Evaluation of OMI upper troposphere NO_2 with aircraft observations

The aircraft observations we use to arbitrate between the OMI NO_2 products are from thermal-dissociation laser-induced fluorescence (TD-LIF) instruments (Day et al., 2002) for NASA DC8 aircraft campaigns over North America and Greenland in spring-summer when there is a high density of measurement campaigns. These include INTEX-A, INTEX-B, ARCTAS, DC3,



140 and SEAC⁴RS. Only INTEX-B is in the same year as the OMI products but we consider interannual variability to be only a small source of error. Measurements of NO₂ from TD-LIF are susceptible to interference from decomposition of thermally unstable reservoir compounds methyl peroxy nitrate (CH₃O₂NO₂) and HNO₄, in particular in the UT, where NO₂ concentrations are relatively low, temperature gradients between the instrument inlet and ambient air are large, and reservoir compounds are abundant (Browne et al., 2011). Publicly available DC3 and SEAC⁴RS TD-LIF NO₂ are already corrected for this interference.

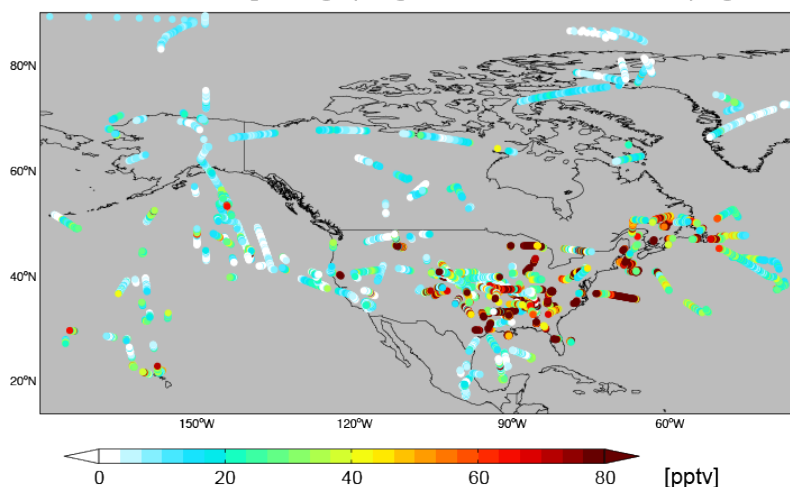
145 We apply a correction for the other campaigns using the relationship between temperature and percentage interference from Browne et al. (2011). Observed mean ambient air temperature in the UT during INTEX-A is 246 K, corresponding to 20% interference. That for INTEX-B is 241 K (30% interference) and 236 K for ARCTAS (38% interference).

There are also NO₂ observations from the recent NASA ATom campaign, and from the In-service Aircraft for a Global

150 Observing System (IAGOS) commercial aircraft campaign (Berkes et al., 2017). These use chemiluminescence instruments that are also susceptible to interference. Chemiluminescence and TD-LIF NO₂ are consistent during the SEAC⁴RS campaign for the altitude range considered in this work (6-9 km) (Travis et al., 2016), but the interference from chemiluminescence is challenging to quantify, due to dependence also on the operator and instrument design that varies across campaigns (Reed et al., 2016).

155 Figure 2 shows the sampling extent of TD-LIF UT NO₂ over North America and Greenland in spring-summer at 450-280 hPa, around the satellite overpass (11h00-16h00 LT) for scenes not influenced by the stratosphere (diagnosed with collocated ozone/CO > 1.25 mol mol⁻¹ (Hudman et al., 2007)). Concentrations of UT NO₂ exceed 80 pptv over the eastern US due to lightning NO_x emissions and are < 30 pptv over the rest of the domain.

TD-LIF UT NO₂ during spring-summer NASA DC8 campaigns



160

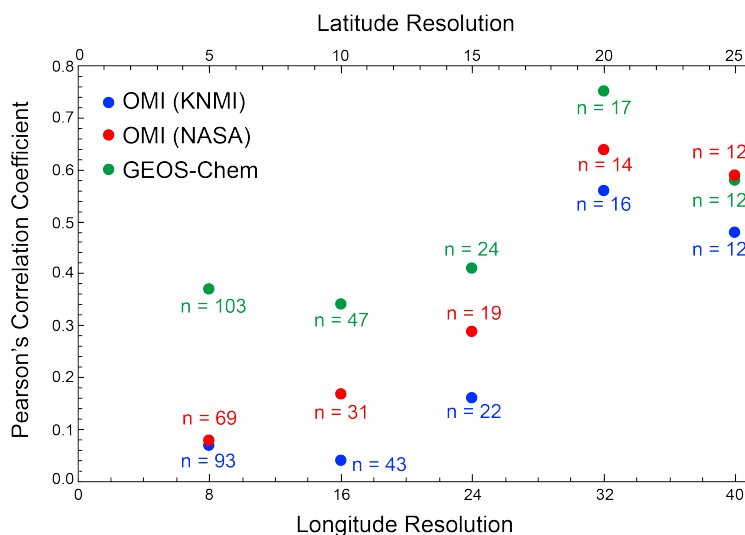
Figure 2. NASA DC8 upper troposphere NO₂ over North America in spring-summer (March–August). Observations are from the TD-LIF instrument at 450–280 hPa, 11h00–16h00 local time, and without stratospheric influence. Campaigns include INTEX-A in June–August 2004 (Singh et al., 2006), INTEX-B in March–May 2006 (Singh et al., 2009), ARCTAS in March–April and June–July 2008 (Jacob et al., 2010), DC3 in May–June 2012 (Barth et al., 2015), and SEAC⁴RS in August 2013 (Toon et al., 2016).

165

Figure 3 shows the spatial correlation between March–August mean gridded aircraft and OMI UT NO₂ from the 2 products as a function of horizontal resolution. There is no spatial consistency between the OMI products and aircraft NO₂ at 5° × 8° (R < 0.1) and 10° × 16° (R < 0.2). The correlation improves for both products with further spatial averaging, peaking at 20° × 32° (R =



0.56 for KNMI, $R = 0.64$ for NASA). The satellite products are also spatially consistent at this resolution over this domain ($R =$
 170 0.89), but KNMI is 43% lower than NASA.

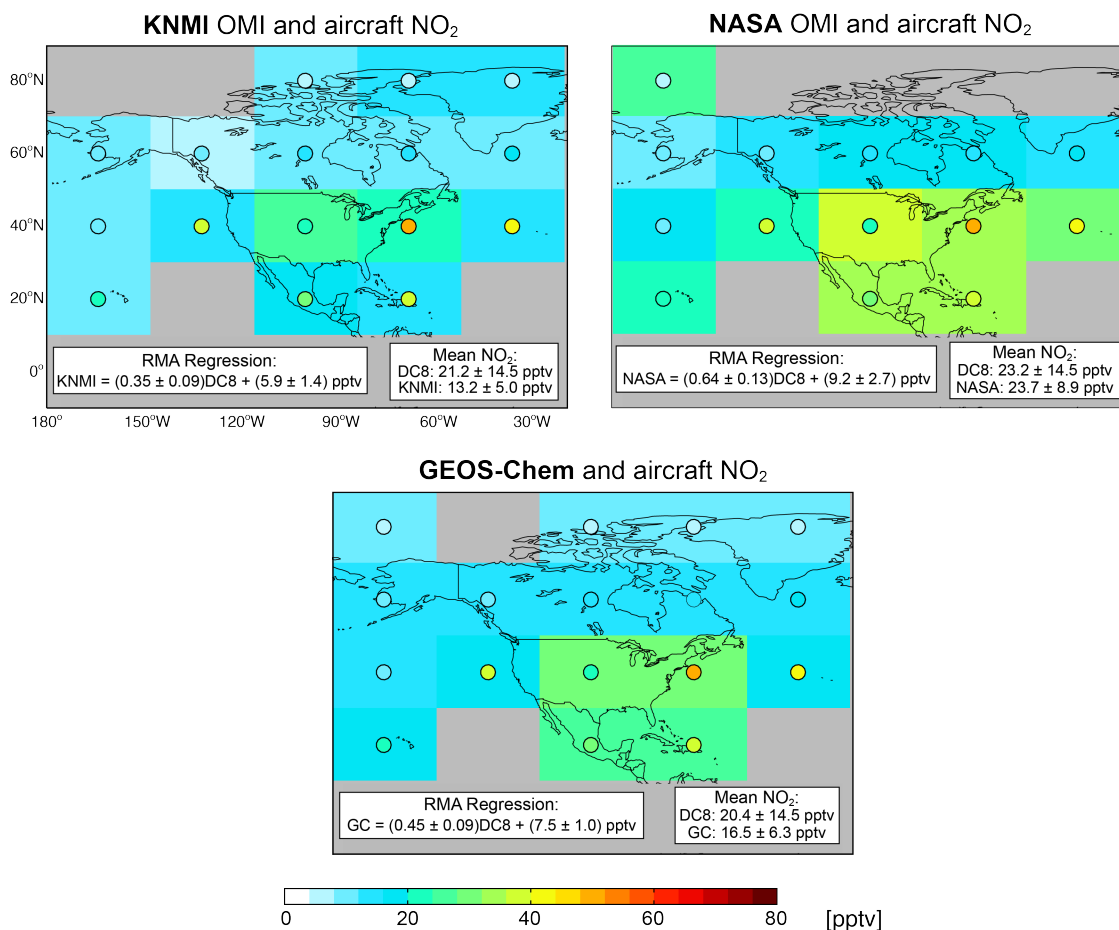


175 **Figure 3. Evaluation of OMI and GEOS-Chem upper troposphere NO_2 with aircraft observations. Individual points are Pearson's correlation coefficients between gridded March–August mean UT NO_2 measured from the aircraft and OMI KNMI in 2006 (blue), OMI NASA in 2005–2007 (red), and GEOS-Chem in 2006 (green) at $5^\circ \times 8^\circ$ (latitude \times longitude), $10^\circ \times 16^\circ$, $15^\circ \times 24^\circ$, $20^\circ \times 32^\circ$, and $25^\circ \times 40^\circ$. Values inset are the number of points at each resolution. The domain sampled is shown in Figure 2.**

Figure 4 compares the spatial distribution of OMI and aircraft UT NO_2 at $20^\circ \times 32^\circ$ over North America. Domain mean KNMI
 180 UT NO_2 is 38% lower than the aircraft observations, compared to 2.2% higher for NASA UT NO_2 . Both products exhibit less
 190 variability (reduced major axis, RMA, regression slopes < 1) and high bias in background NO_2 compared to the aircraft
 observations (positive RMA intercepts of 5.9 ± 1.4 pptv for KNMI and 9.2 ± 2.7 pptv for NASA). We proceed with the NASA
 UT NO_2 product at $20^\circ \times 32^\circ$, as correlation peaks at this resolution and the NASA product is more consistent with domain mean
 aircraft UT NO_2 than the KNMI product.

4. Constraints on upper tropospheric NO_x

185 The NASA product provides near-global coverage of UT NO_2 to assess current understanding of regional UT NO_x sources and
 dynamics by comparing to UT NO_2 from the GEOS-Chem CTM (version 10-01; http://wiki.seas.harvard.edu/geos-chem/index.php/GEOS-Chem_v10-01) driven with NASA MERRA-2 reanalysis meteorology. The model horizontal resolution
 is $2^\circ \times 2.5^\circ$ and the output is regridded to $20^\circ \times 32^\circ$ for comparison with OMI. GEOS-Chem is sampled under all-sky conditions.
 We find that the effect on NO_2 of sampling the model under cloudy conditions is small. Isolating NO_2 under very cloudy
 190 conditions using MERRA-2 cloud fractions decreases modeled UT NO_2 by no more than 5 pptv in the tropics/subtropics and less
 at higher latitudes. We use output from the model for 2006 following a one-year spin-up for chemical initialization. Interannual
 variability in UT NO_2 , determined as the difference between modeled 2006 and multi-year (mean 2005–2007) UT NO_2 , is small
 (< 4 pptv) everywhere except central Africa year-round (4–12 pptv), the Arctic north of 60°N (up to 25 pptv), and the Middle
 East in June–August and northern India in March–May (both 10–20 pptv).



195

Figure 4. March-August upper troposphere NO₂ over North America. All data are at 20° × 32°. Background colors in the different panels show concentrations from KNMI, NASA, and GEOS-Chem (GC). Circles show the aircraft observations (same in all panels). Aircraft observations are for 11h00-16h00 LT. The model is sampled in the satellite overpass time window (12h00-15h00 LT). Model and aircraft data are at 280-450 hPa and screened for stratospheric influence using ozone/CO > 1.25 mol mol⁻¹. Inset boxes show reduced major axis (RMA) regression statistics and mean NO₂ for coincident gridsquares. Grey gridsquares indicate no observations.

200

Emission sources of UT NO_x include aircraft emissions and lightning conversion of N₂ and O₂ to reactive NO_x. In the model, global aircraft emissions in the model from the AEIC inventory (Stettler et al., 2011) total 0.82 Tg N in 2006; much less than lightning in the same year (6.5 Tg N). Lightning in the model is estimated using the parameterization implemented by Murray et al. (2012). This includes an initial estimate of lightning flashes using the Price and Rind (1992, 1993, 1994) relationship between cloud-top height and lightning flashes. These are then scaled to the same annual global flash frequency (46 fl s⁻¹) as the climatology from the combined Lightning Imaging Sensor (LIS) and Optical Transient Detector (OTD) high-resolution monthly climatology (LIS/OTD HRMC) (Cecil et al., 2014). LIS/OTD is used again to redistribute lightning flashes horizontally to match the location of lightning flashes in the satellite monthly climatology. Flashes are assigned production rates of 500 mol N fl⁻¹ in the northern midlatitudes (north of 35°N) and 260 mol N fl⁻¹ everywhere else. The resultant lightning NO_x emissions are distributed vertically from the surface to the top of clouds using regional vertical profiles from Ott et al. (2010). We find that GEOS-Chem overestimates UT NO₂ in summer across the northern midlatitudes by 10-20 pptv (not shown) compared to OMI

210



that we attribute to excessive lightning NO_x emissions. We correct for this overestimate by instead using a single global NO_x production rate of $260 \text{ mol N fl}^{-1}$ in the model. This decreases global lightning NO_x emissions by 15% from 6.5 to 5.5 Tg N a^{-1} .

215

Figure 3 shows the spatial correlation between the model and aircraft observations. The model is more consistent with the aircraft observations than OMI at fine spatial resolution. Like OMI, GEOS-Chem correlation with the aircraft observations improves with spatial averaging, peaking at $20^\circ \times 32^\circ$ ($R = 0.75$). Figure 4 also shows comparison of March-August GEOS-Chem UT NO_2 with the aircraft observations at $20^\circ \times 32^\circ$. The model is sampled over the same pressure range as NASA (280-450 hPa) around the OMI overpass (12h00-15h00 LT) and is filtered for stratospheric influence using model ozone/ $\text{CO} > 1.25 \text{ mol mol}^{-1}$. Domain average UT NO_2 from the model is 19% lower than the aircraft measurements and the model also overestimates background UT NO_2 (intercept = $7.5 \pm 1.0 \text{ pptv}$) and underestimates the variability (slope = 0.45 ± 0.09).

Figure 5 compares seasonal mean OMI and GEOS-Chem UT NO_2 in December-February and June-August. Formation of PAN, HNO_4 and $\text{CH}_3\text{O}_2\text{NO}_2$ is the dominant loss pathway for NO_2 in all seasons ($>75\%$ branching ratio), according to GEOS-Chem. Lower UT NO_2 in the northern hemisphere winter compared to summer in the model is because lightning activity is at a minimum and there is reduced formation of NO_2 from thermal decomposition of PAN and photolysis of PAN and HNO_3 . The model underestimates UT NO_2 in the northern midlatitudes in winter by 20-40 pptv, suggesting misrepresentation of another process in the model or contamination of OMI UT NO_2 from NO_2 below clouds. The latter effect is likely to be worst over polluted regions in winter when NO_2 at the surface is long-lived and abundant.

230

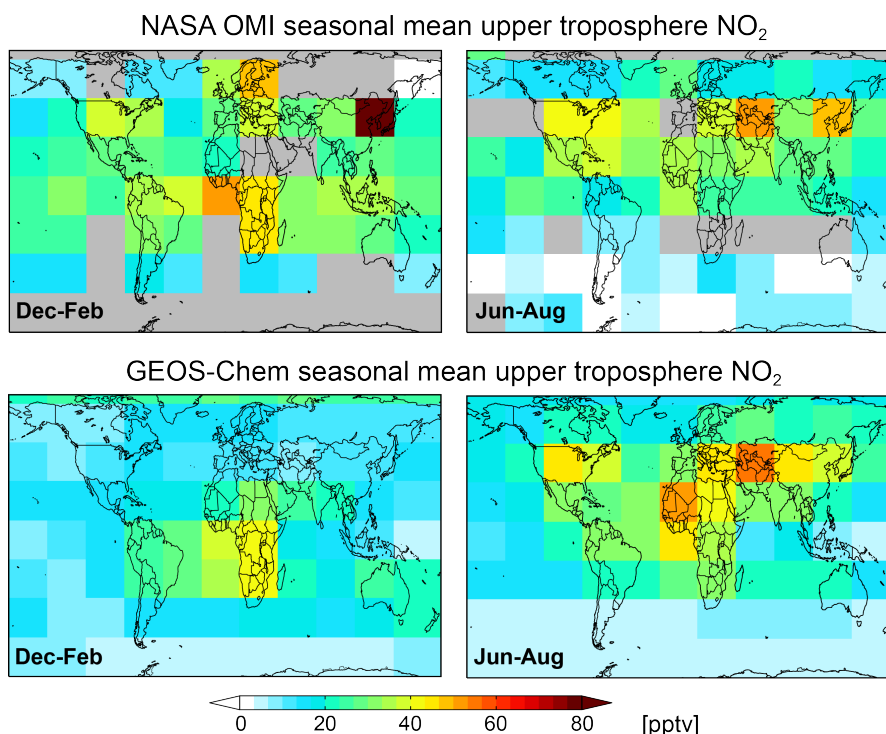


Figure 5. Observed and modelled upper troposphere NO_2 . NASA OMI for 2005-2007 (top) and GEOS-Chem (bottom) seasonal mean UT NO_2 . The model is sampled at 280-450 hPa during the satellite overpass (12h00-15h00 LT), and filtered for stratospheric influence. Data are at $20^\circ \times 32^\circ$ horizontal resolution for December-February (left) and June-August (right). Grey gridsquares in the top panel indicate no OMI data.

235



Figure 6 shows the relationship between seasonal mean LIS/OTD lightning flash climatology and seasonal mean UT NO₂ from OMI and GEOS-Chem. Data are divided into seasonal means for the northern mid-latitudes and tropics. OMI UT NO₂ and lightning flashes are spatially consistent ($R > 0.5$) and slopes for the northern mid-latitudes and the tropics are similar, providing
 240 no support for the previously reported higher lightning NO_x production rates in the mid-latitudes than the tropics (Schumann and Huntrieser, 2007; Ott et al., 2010; Laughner and Cohen, 2017; Nault et al., 2017). NO₂ varies with the log of lightning frequency, suggesting faster NO_x loss and shorter NO_x lifetime at high lightning frequencies. The model deviates from the observed log-linear relationship at low lightning frequencies either due to too fast NO_x loss or because the observations are uncertain at low concentrations of NO₂.

245

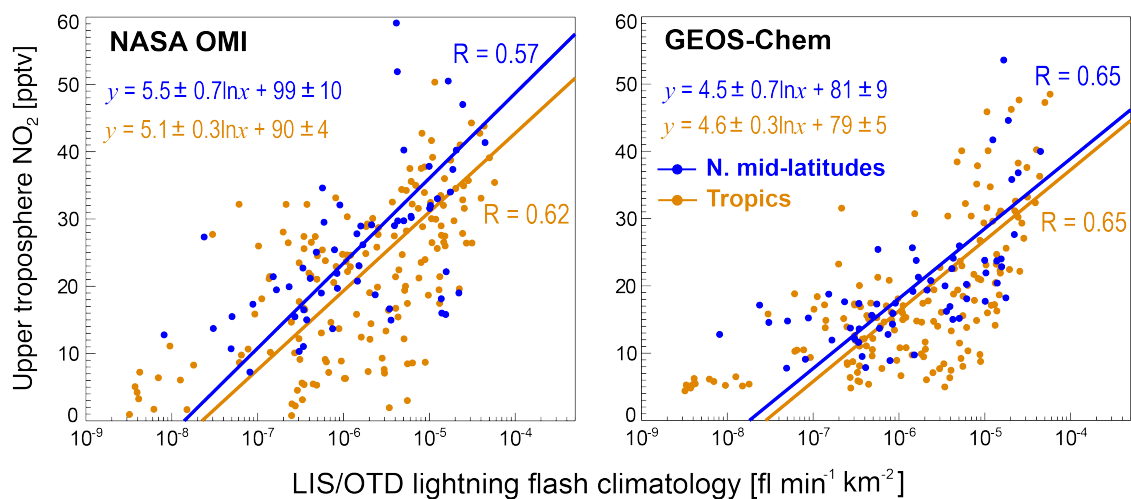


Figure 6. Spatial consistency between upper troposphere NO₂ and lightning flash frequencies. Individual points are seasonal mean UT NO₂ from OMI (left) and GEOS-Chem (right) versus seasonal mean LIS/OTD lightning flash climatologies for coincident 20° × 32° gridsquares in the northern midlatitudes (> 30°N; blue) and tropics (< 30°N; orange). Northern mid-latitude points exclude December-February that show poor correlation with lightning flashes (see text for details). Values inset are Pearson's correlation coefficients and RMA regression statistics.

The northern mid-latitudes data points in Figure 6 exclude December-February, when lightning is at a minimum and correlation between NO₂ and lightning flashes is weak ($R = 0.33$). Results from multi-model sensitivity studies indicate UT NO_x is then predominantly from surface sources, with a smaller contribution from extra-tropical lightning (Grewe et al., 2001). The model
 255 reproduces the observed slopes in Figure 6. Spatial correlation between OMI and LIS/OTD suggests that OMI UT NO₂ can be used to derive spatially and seasonally varying lightning NO_x production rates per flash by scaling 260 mol N fl⁻¹ by the local ratio of observed-to-modelled (OMI/GEOS-Chem) UT NO₂.

Figure 7 shows the resultant seasonal mean OMI-derived lightning NO_x production rates at 20° × 32°. Production rates vary from
 260 100 to 900 mol N fl⁻¹. The largest deviation from 260 mol fl⁻¹ is in Southeast Asia year-round. OMI-derived lightning NO_x production rates are lower over North America in summer (269 mol N fl⁻¹) than autumn (379 mol N fl⁻¹), similar to the generally lower production rates estimated from aircraft observations in Colorado in July (21-465 mol N fl⁻¹) compared to September (481-1445 mol N fl⁻¹) (Schumann and Huntrieser, 2007). A large range in NO_x production rates is obtained from field experiments in the tropics (23-814 mol N fl⁻¹) and mid-latitudes (21-1445 mol N fl⁻¹). Models often assume higher production rates in the mid-latitudes than the tropics (Hudman et al., 2007; Ott et al., 2010; Murray et al., 2012), whereas values estimated using OMI are
 265



270

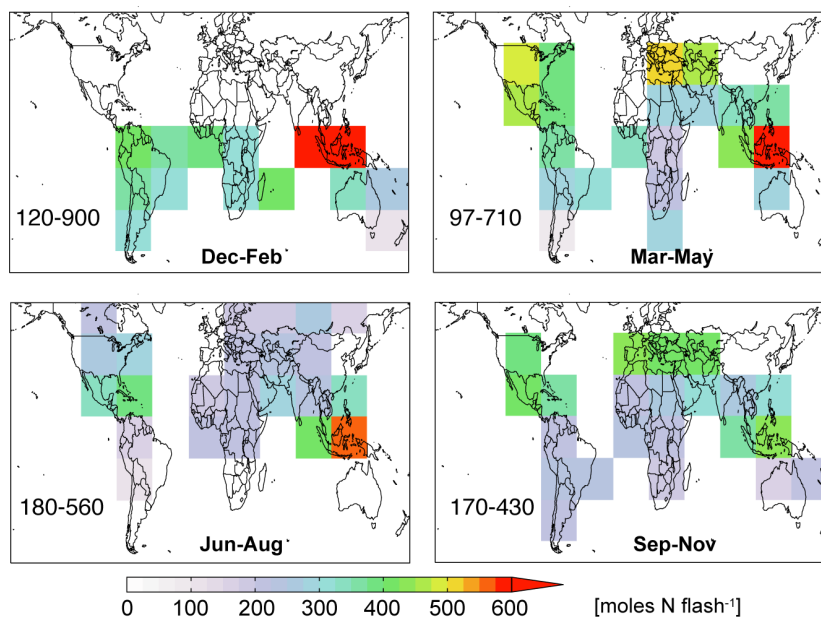
 OMI-derived seasonal mean lightning NO_x production rates


Figure 7. Lightning NO_x production rates per flash estimated with OMI and GEOS-Chem. Maps show seasonal mean nitrogen (N) produced per flash at $20^\circ \times 32^\circ$ for gridsquares with lightning flashes $> 5 \times 10^{-6}$ flashes $\text{km}^{-2} \text{min}^{-1}$. Values inset are the range in production rates for each season. White gridsquares remain unchanged ($260 \text{ mol N fl}^{-1}$).

275

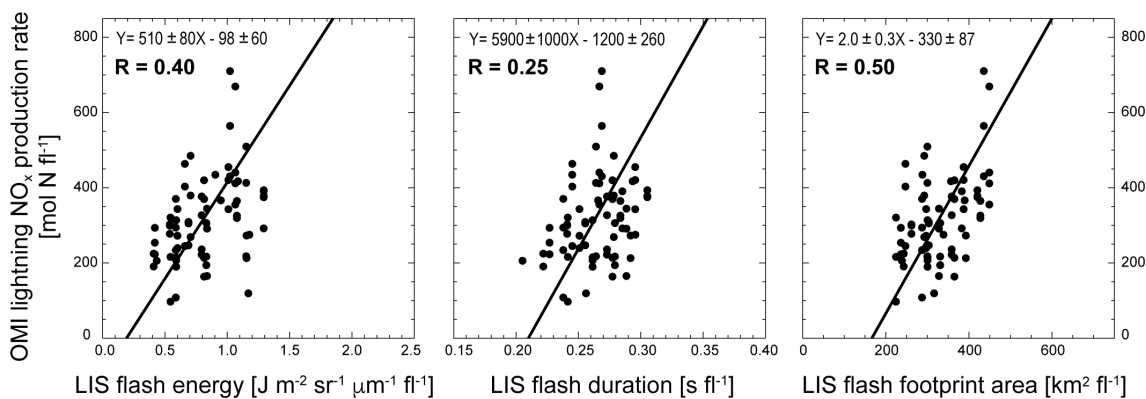


Figure 8. Relationship between OMI-derived lightning NO_x production rates and LIS lightning properties: energy (radiance), duration, and footprint area. Individual points are seasonal means at $20^\circ \times 32^\circ$ from Figure 7 at 40°N - 40°S .

Properties of lightning flashes, including energy, duration and footprint area, have been retrieved from the OTD and LIS sensors (Beirle et al., 2014). The flash footprint area is the spatial extent of lightning detection events contributing to the flash (collection



of local events) diagnosed by the satellite data. Figure 8 shows the relationship between OMI-derived lightning NO_x production rates from Figure 7 and LIS lightning properties from Beirle et al. (2014). The strongest correlation is with lightning extent ($R = 0.50$), followed by energy ($R = 0.40$). The correlation with flash duration is weak ($R = 0.25$). The relationships in Figure 8 suggest a dependence of lightning NO_x production rates on lightning flash energy of $510 \pm 80 \text{ mol N (J m}^{-2} \text{ sr}^{-1} \mu\text{m}^{-1})^{-1}$ and on flash footprint area of $2.0 \pm 0.3 \text{ mol N km}^{-2}$. OMI-derived NO_x production rates in Figure 7 and lightning flash interannual variability from LIS applied to GEOS-Chem yield global lightning NO_x emission of 5.6 Tg N a^{-1} .

5. Conclusions

290 The majority of measurements of NO_x in the upper troposphere (UT) are from measurement campaigns that are limited in space and time. Two new UT NO_2 products from the Ozone Monitoring Instrument (OMI) offer the potential to address uncertainties in our understanding of UT NO_x sources. We intercompare these products, use aircraft observations to arbitrate, and test the potential to constrain UT NO_x sources using the GEOS-Chem model.

295 The OMI UT NO_2 products use different retrieval methods to obtain distinct and inconsistent ($R < 0.5$) NO_2 mixing ratios in the UT ($\sim 280\text{--}450 \text{ hPa}$). The product retrieved by NASA is more consistent with aircraft observations of NO_2 for spring-summer over North America than the product retrieved by KNMI and offers information about seasonal UT NO_2 at very coarse spatial scales ($20^\circ \times 32^\circ$; latitude \times longitude).

300 The majority of the spatial variability in OMI UT NO_2 can be attributed to lightning, except in the northern midlatitudes in winter. A similar relationship between UT NO_2 and lightning flashes from the LIS/OTD climatology in the tropics and northern mid-latitudes offers no support for higher lightning NO_x production rates in the northern mid-latitudes than the tropics. We derive a global mean lightning NO_x production rate of $280 \text{ mol N fl}^{-1}$ and estimate global lightning NO_x emissions of 5.6 Tg N for 2006.

305 Data Availability

Data from this work can be made available upon request to E. A. Marais for GEOS-Chem output, M. Belmonte-Rivas for KNMI UT NO_2 , and S. Choi and J. Joiner for NASA OMI UT NO_2 , and S. Beirle for LIS lightning properties.

Competing Interests

The authors declare that they have no conflicts of interest.

310 Acknowledgements

This work was funded by the NASA Tropospheric Chemistry Program and a University of Birmingham Research Fellowship awarded to EAM. Model simulations were performed on the University of Birmingham's BlueBEAR High Performance Cluster. The authors would like to thank the BlueBEAR support team for IT and HPC support.

References



- 315 Acarreta, J. R., De Haan, J. F., and Stammes, P.: Cloud pressure retrieval using the O₂-O₂ absorption band at 477 nm, *J. Geophys. Res.*, 109, doi:10.1029/2003jd003915, 2004.
- Allen, D., Pickering, K., Duncan, B., and Damon, M.: Impact of lightning NO emissions on North American photochemistry as determined using the Global Modeling Initiative (GMI) model, *J. Geophys. Res.*, 115, doi:10.1029/2010jd014062, 2010.
- 320 Baehr, J., Schlager, H., Ziereis, H., Stock, P., van Velthoven, P., Busen, R., Strom, J., and Schumann, U.: Aircraft observations of NO, NO_y, CO, and O₃ in the upper troposphere from 60°N to 60°S - Interhemispheric differences at midlatitudes, *Geophys. Res. Lett.*, 30, doi:10.1029/2003gl016935, 2003.
- Barth, M. C., Cantrell, C. A., Brune, W. H., Rutledge, S. A., Crawford, J. H., Huntrieser, H., Carey, L. D., MacGorman, D., Weisman, M., Pickering, K. E., Bruning, E., Anderson, B., Apel, E., Biggerstaff, M., Campos, T., Campuzano-Jost, P., Cohen, R., Crouse, J., Day, D. A., Diskin, G., Flocke, F., Fried, A., Garland, C., Heikes, B., Honomichl, S., Hornbrook, R., Huey, L. G., Jimenez, J. L., Lang, T., Lichtenstern, M., Mikoviny, T., Nault, B., O'Sullivan, D., Pan, L. L., Peischl, J., Pollack, I., Richter, D., Riemer, D., Ryerson, T., Schlager, H., St Clair, J., Walega, J., Weibring, P., Weinheimer, A., Wennberg, P., Wisthaler, A., Wooldridge, P. J., and Ziegler, C.: The Deep Convective Clouds and Chemistry (DC3) Field Campaign, *B. Am. Meteorol. Soc.*, 96, 1281-1309, doi:10.1175/Bams-D-13-00290.1, 2015.
- 325 Belmonte-Rivas, M. B., Veeffkind, P., Boersma, F., Levelt, P., Eskes, H., and Gille, J.: Intercomparison of daytime stratospheric NO₂ satellite retrievals and model simulations, *Atmos. Meas. Tech.*, 7, 2203-2225, doi:10.5194/amt-7-2203-2014, 2014.
- 330 Belmonte-Rivas, M. B., Veeffkind, P., Eskes, H., and Levelt, P.: OMI tropospheric NO₂ profiles from cloud slicing: constraints on surface emissions, convective transport and lightning NO_x, *Atmos. Chem. Phys.*, 15, 13519-13553, doi:10.5194/acp-15-13519-2015, 2015.
- Berkes, F., Houben, N., Bundke, U., Franke, H., Pätz, H.-W., Rohrer, F., Wahner, A., and Petzold, A.: The IAGOS NO_x Instrument – Design, operation and first results from deployment aboard passenger aircraft, *Atmos. Meas. Tech.*, doi:10.5194/amt-2017-435, 2017.
- 335 Bertram, T. H., Perring, A. E., Wooldridge, P. J., Crouse, J. D., Kwan, A. J., Wennberg, P. O., Scheuer, E., Dibb, J., Avery, M., Sachse, G., Vay, S. A., Crawford, J. H., McNaughton, C. S., Clarke, A., Pickering, K. E., Fuelberg, H., Huey, G., Blake, D. R., Singh, H. B., Hall, S. R., Shetter, R. E., Fried, A., Heikes, B. G., and Cohen, R. C.: Direct measurements of the convective recycling of the upper troposphere, *Science*, 315, 816-820, doi:10.1126/science.1134548, 2007.
- 340 Boersma, K. F., Eskes, H. J., Dirksen, R. J., van der A, R. J., Veeffkind, J. P., Stammes, P., Huijnen, V., Kleipool, Q. L., Sneep, M., Claas, J., Leitao, J., Richter, A., Zhou, Y., and Brunner, D.: An improved tropospheric NO₂ column retrieval algorithm for the Ozone Monitoring Instrument, *Atmos. Meas. Tech.*, 4, 1905-1928, doi:10.5194/amt-4-1905-2011, 2011.
- Bradshaw, J., Davis, D., Grodzinsky, G., Smyth, S., Newell, R., Sandholm, S., and Liu, S.: Observed distributions of nitrogen oxides in the remote free troposphere from the NASA global tropospheric experiment programs, *Rev. Geophys.*, 38, 61-116, doi:10.1029/1999rg900015, 2000.
- 345 Browne, E. C., Perring, A. E., Wooldridge, P. J., Apel, E., Hall, S. R., Huey, L. G., Mao, J., Spencer, K. M., St Clair, J. M., Weinheimer, A. J., Wisthaler, A., and Cohen, R. C.: Global and regional effects of the photochemistry of CH₃O₂NO₂: evidence from ARCTAS, *Atmos. Chem. Phys.*, 11, 4209-4219, doi:10.5194/acp-11-4209-2011, 2011.
- 350 Brunner, D., Staehelin, J., Jeker, D., Wernli, H., and Schumann, U.: Nitrogen oxides and ozone in the tropopause region of the Northern Hemisphere: Measurements from commercial aircraft in 1995/1996 and 1997, *J. Geophys. Res.*, 106, 27673-27699, doi:10.1029/2001jd900239, 2001.
- Cecil, D. J., Buechler, D. E., and Blakeslee, R. J.: Gridded lightning climatology from TRMM-LIS and OTD: Dataset description, *Atmos. Res.*, 135, 404-414, doi:10.1016/j.atmosres.2012.06.028, 2014.
- 355 Choi, S., Joiner, J., Choi, Y., Duncan, B. N., Vasilkov, A., Krotkov, N., and Bucsela, E.: First estimates of global free-tropospheric NO₂ abundances derived using a cloud-slicing technique applied to satellite observations from the Aura Ozone Monitoring Instrument (OMI), *Atmos. Chem. Phys.*, 14, 10565-10588, doi:10.5194/acp-14-10565-2014, 2014.
- Crawford, J. H., Davis, D. D., Chen, G., Bradshaw, J., Sandholm, S., Kondo, Y., Merrill, J., Liu, S., Browell, E., Gregory, G., Anderson, B., Sachse, G., Barrick, J., Blake, D., Talbot, R., and Poeschel, R.: Implications of large scale shifts in tropospheric NO_x levels in the remote tropical Pacific, *J. Geophys. Res.*, 102, 28447-28468, doi:10.1029/97jd00011, 1997.
- 360 Dahlmann, K., Grewe, V., Ponater, M., and Matthes, S.: Quantifying the contributions of individual NO_x sources to the trend in ozone radiative forcing, *Atmos. Environ.*, 45, 2860-2868, doi:10.1016/j.atmosenv.2011.02.071, 2011.
- Day, D. A., Wooldridge, P. J., Dillon, M. B., Thornton, J. A., and Cohen, R. C.: A thermal dissociation laser-induced fluorescence instrument for in situ detection of NO₂, peroxy nitrates, alkyl nitrates, and HNO₃, *J. Geophys. Res.*, 107, doi:10.1029/2001jd000779, 2002.
- 365 Denman, K. L., and Brasseur, G.: Couplings between changes in the climate system and biogeochemistry, In: *Climate Change 2007: The Physical Science Basis. Contribution of Working Group I to the Fourth Assessment Report of the Intergovernmental Panel on Climate Change*, edited by: Solomon, S., Qin, D., Manning, M., Chen, Z., Marquis, M., Averyt, K. B., Tignor, M., and Miller, H. L., Cambridge University Press, Cambridge, UK, 499-587, 2007.
- 370 Drummond, J. W., Ehhalt, D. H., and Volz, A.: Measurements of nitric oxide between 0-12 km altitude and 67°N to 60°S latitude obtained during STRATOZ III, *J. Geophys. Res.*, 93, 15831-15849, doi:10.1029/JD093iD12p15831, 1988.



- Ehhalt, D. H., Rohrer, F., and Wahner, A.: Sources and distribution of NO_x in the upper troposphere at northern midlatitudes, *J. Geophys. Res.*, **97**, 3725-3738, doi:10.1029/91JD03081, 1992.
- 375 Finney, D. L., Doherty, R. M., Wild, O., Huntrieser, H., Pumphrey, H. C., and Blyth, A. M.: Using cloud ice flux to parametrise large-scale lightning, *Atmos. Chem. Phys.*, **14**, 12665-12682, doi:10.5194/acp-14-12665-2014, 2014.
- Finney, D. L., Doherty, R. M., Wild, O., Young, P. J., and Butler, A.: Response of lightning NO_x emissions and ozone production to climate change: Insights from the Atmospheric Chemistry and Climate Model Intercomparison Project, *Geophys. Res. Lett.*, **43**, 5492-5500, doi:10.1002/2016gl068825, 2016.
- 380 Finney, D. L., Doherty, R. M., Wild, O., Stevenson, D. S., MacKenzie, I. A., and Blyth, A. M.: A projected decrease in lightning under climate change, *Nat. Clim. Change*, **8**, 210-213, doi:10.1038/s41558-018-0072-6, 2018.
- Grewe, V., Brunner, D., Dameris, M., Grenfell, J. L., Hein, R., Shindell, D., and Staehelin, J.: Origin and variability of upper tropospheric nitrogen oxides and ozone at northern mid-latitudes, *Atmos. Environ.*, **35**, 3421-3433, doi:10.1016/S1352-2310(01)00134-0, 2001.
- 385 Hudman, R. C., Jacob, D. J., Turquety, S., Leibensperger, E. M., Murray, L. T., Wu, S., Gilliland, A. B., Avery, M., Bertram, T. H., Brune, W., Cohen, R. C., Dibb, J. E., Flocke, F. M., Fried, A., Holloway, J., Neuman, J. A., Orville, R., Perring, A., Ren, X., Sachse, G. W., Singh, H. B., Swanson, A., and Wooldridge, P. J.: Surface and lightning sources of nitrogen oxides over the United States: Magnitudes, chemical evolution, and outflow, *J. Geophys. Res.*, **112**, doi:10.1029/2006jd007912, 2007.
- 390 Jacob, D. J., Heikes, B. G., Fan, S. M., Logan, J. A., Mauzerall, D. L., Bradshaw, J. D., Singh, H. B., Gregory, G. L., Talbot, R. W., Blake, D. R., and Sachse, G. W.: Origin of ozone and NO_x in the tropical troposphere: A photochemical analysis of aircraft observations over the South Atlantic basin, *J. Geophys. Res.*, **101**, 24235-24250, doi:10.1029/96jd00336, 1996.
- Jacob, D. J., Crawford, J. H., Maring, H., Clarke, A. D., Dibb, J. E., Emmons, L. K., Ferrare, R. A., Hostetler, C. A., Russell, P. B., Singh, H. B., Thompson, A. M., Shaw, G. E., McCauley, E., Pederson, J. R., and Fisher, J. A.: The Arctic Research of the Composition of the Troposphere from Aircraft and Satellites (ARCTAS) mission: design, execution, and first results, *Atmos. Chem. Phys.*, **10**, 5191-5212, doi:10.5194/acp-10-5191-2010, 2010.
- 395 Jaeglé, L., Jacob, D. J., Brune, W. H., Tan, D., Faloon, I. C., Weinheimer, A. J., Ridley, B. A., Campos, T. L., and Sachse, G. W.: Sources of HO_x and production of ozone in the upper troposphere over the United States, *Geophys. Res. Lett.*, **25**, 1709-1712, doi:10.1029/98gl00041, 1998a.
- 400 Jaeglé, L., Jacob, D. J., Wang, Y., Weinheimer, A. J., Ridley, B. A., Campos, T. L., Sachse, G. W., and Hagen, D. E.: Sources and chemistry of NO_x in the upper troposphere over the United States, *Geophys. Res. Lett.*, **25**, 1705-1708, doi:10.1029/97gl03591, 1998b.
- Krotkov, N. A., Lamsal, L. N., Celarier, E. A., Swartz, W. H., Marchenko, S. V., Bucsela, E. J., Chan, K. L., Wenig, M., and Zara, M.: The version 3 OMI NO₂ standard product, *Atmos. Meas. Tech.*, **10**, 3133-3149, doi:10.5194/amt-10-3133-2017, 2017.
- 405 Laughner, J. L., and Cohen, R. C.: Quantification of the effect of modeled lightning NO₂ on UV-visible air mass factors, *Atmos. Meas. Tech.*, **10**, 4403-4419, doi:10.5194/amt-10-4403-2017, 2017.
- Levelt, P. F., Van den Oord, G. H. J., Dobber, M. R., Malkki, A., Visser, H., de Vries, J., Stammes, P., Lundell, J. O. V., and Saari, H.: The Ozone Monitoring Instrument, *IEEE T. Geosci. Remote*, **44**, 1093-1101, doi:10.1109/Tgrs.2006.872333, 2006.
- 410 Marchenko, S., Krotkov, N. A., Lamsal, L. N., Celarier, E. A., Swartz, W. H., and Bucsela, E. J.: Revising the slant column density retrieval of nitrogen dioxide observed by the Ozone Monitoring Instrument, *J. Geophys. Res.*, **120**, 5670-5692, doi:10.1002/2014jd022913, 2015.
- Miyazaki, K., Eskes, H. J., Sudo, K., and Zhang, C.: Global lightning NO_x production estimated by an assimilation of multiple satellite data sets, *Atmos. Chem. Phys.*, **14**, 3277-3305, doi:10.5194/acp-14-3277-2014, 2014.
- 415 Murray, L. T., Jacob, D. J., Logan, J. A., Hudman, R. C., and Koshak, W. J.: Optimized regional and interannual variability of lightning in a global chemical transport model constrained by LIS/OTD satellite data, *J. Geophys. Res.*, **117**, doi:10.1029/2012jd017934, 2012.
- Murray, L. T., Mickley, L. J., Kaplan, J. O., Sofen, E. D., Pfeiffer, M., and Alexander, B.: Factors controlling variability in the oxidative capacity of the troposphere since the Last Glacial Maximum, *Atmos. Chem. Phys.*, **14**, 3589-3622, doi:10.5194/acp-14-3589-2014, 2014.
- 420 Murray, L. T.: Lightning NO_x and Impacts on Air Quality, *Current Pollution Reports*, **2**, 115-133, doi:10.1007/s40726-016-0031-7, 2016.
- Nault, B. A., Garland, C., Wooldridge, P. J., Brune, W. H., Campuzano-Jost, P., Crouse, J. D., Day, D. A., Dibb, J., Hall, S. R., Huey, L. G., Jimenez, J. L., Liu, X. X., Mao, J. Q., Mikoviny, T., Peischl, J., Pollack, I. B., Ren, X. R., Ryerson, T. B., Scheuer, E., Ullmann, K., Wennberg, P. O., Wisthaler, A., Zhang, L., and Cohen, R. C.: Observational Constraints on the Oxidation of NO_x in the Upper Troposphere, *J. Phys. Chem. A*, **120**, 1468-1478, doi:10.1021/acs.jpca.5b07824, 2016.



- Nault, B. A., Laughner, J. L., Wooldridge, P. J., Crouse, J. D., Dibb, J., Diskin, G., Peischl, J., Podolske, J. R., Pollack, I. B., Ryerson, T. B., Scheuer, E., Wennberg, P. O., and Cohen, R. C.: Lightning NO_x Emissions: Reconciling Measured and Modeled Estimates With Updated NO_x Chemistry, *Geophys. Res. Lett.*, 44, 9479-9488, doi:10.1002/2017gl074436, 2017.
- 430 Ott, L. E., Pickering, K. E., Stenchikov, G. L., Allen, D. J., DeCaria, A. J., Ridley, B., Lin, R. F., Lang, S., and Tao, W. K.: Production of lightning NO_x and its vertical distribution calculated from three-dimensional cloud-scale chemical transport model simulations, *J. Geophys. Res.*, 115, doi:10.1029/2009jd011880, 2010.
- Prather, M. J., and Jacob, D. J.: A persistent imbalance in HO_x and NO_x photochemistry of the upper troposphere driven by deep tropical convection, *Geophys. Res. Lett.*, 24, 3189-3192, doi:10.1029/97gl03027, 1997.
- 435 Price, C., and Rind, D.: A simple lightning parameterization for calculating global lightning distributions, *J. Geophys. Res.*, 97, 9919-9933, doi:10.1029/92JD00719, 1992.
- Price, C., and Rind, D.: What determines the cloud-to-ground lightning fraction in thunderstorms, *Geophys. Res. Lett.*, 20, 463-466, doi:10.1029/93gl00226, 1993.
- Price, C., and Rind, D.: Modeling global lightning distributions in a General-Circulation Model, *Mon. Weather Rev.*, 122, 1930-1939, doi:10.1175/1520-0493(1994)122<1930:Mglidia>2.0.Co;2, 1994.
- 440 Rap, A., Richards, N. A. D., Forster, P. M., Monks, S. A., Arnold, S. R., and Chipperfield, M. P.: Satellite constraint on the tropospheric ozone radiative effect, *Geophys. Res. Lett.*, 42, 5074-5081, doi:10.1002/2015gl064037, 2015.
- Reed, C., Evans, M. J., Di Carlo, P., Lee, J. D., and Carpenter, L. J.: Interferences in photolytic NO₂ measurements: explanation for an apparent missing oxidant?, *Atmos. Chem. Phys.*, 16, 4707-4724, doi:10.5194/acp-16-4707-2016, 2016.
- 445 Sauvage, B., Martin, R. V., van Donkelaar, A., Liu, X., Chance, K., Jaeglé, L., Palmer, P. I., Wu, S., and Fu, T. M.: Remote sensed and in situ constraints on processes affecting tropical tropospheric ozone, *Atmos. Chem. Phys.*, 7, 815-838, doi:10.5194/acp-7-815-2007, 2007.
- Schumann, U., and Huntrieser, H.: The global lightning-induced nitrogen oxides source, *Atmos. Chem. Phys.*, 7, 3823-3907, doi:10.5194/acp-7-3823-2007, 2007.
- 450 Singh, H. B., Brune, W. H., Crawford, J. H., Jacob, D. J., and Russell, P. B.: Overview of the summer 2004 intercontinental chemical transport experiment - North America (INTEX-A), *J. Geophys. Res.*, 111, doi:10.1029/2006jd007905, 2006.
- Singh, H. B., Brune, W. H., Crawford, J. H., Flocke, F., and Jacob, D. J.: Chemistry and transport of pollution over the Gulf of Mexico and the Pacific: spring 2006 INTEX-B campaign overview and first results, *Atmos. Chem. Phys.*, 9, 2301-2318, doi:10.5194/acp-9-2301-2009, 2009.
- 455 Stettler, M. E. J., Eastham, S., and Barrett, S. R. H.: Air quality and public health impacts of UK airports. Part I: Emissions, *Atmos. Environ.*, 45, 5415-5424, doi:10.1016/j.atmosenv.2011.07.012, 2011.
- Stratmann, G., Ziereis, H., Stock, P., Brenninkmeijer, C. A. M., Zahn, A., Rauthe-Schoch, A., Velthoven, P. V., Schlager, H., and Volz-Thomas, A.: NO and NO_y in the upper troposphere: Nine years of CARIBIC measurements onboard a passenger aircraft, *Atmos. Environ.*, 133, 93-111, doi:10.1016/j.atmosenv.2016.02.035, 2016.
- 460 Toon, O. B., Maring, H., Dibb, J., Ferrare, R., Jacob, D. J., Jensen, E. J., Luo, Z. J., Mace, G. G., Pan, L. L., Pfister, L., Rosenlof, K. H., Redemann, J., Reid, J. S., Singh, H. B., Thompson, A. M., Yokelson, R., Minnis, P., Chen, G., Jucks, K. W., and Pszenny, A.: Planning, implementation, and scientific goals of the Studies of Emissions and Atmospheric Composition, Clouds and Climate Coupling by Regional Surveys (SEAC⁴RS) field mission, *J. Geophys. Res.*, 121, 4967-5009, doi:10.1002/2015jd024297, 2016.
- 465 Tost, H., Jockel, P. J., and Lelieveld, J.: Lightning and convection parameterisations - uncertainties in global modelling, *Atmos. Chem. Phys.*, 7, 4553-4568, doi:10.5194/acp-7-4553-2007, 2007.
- Travis, K. R., Jacob, D. J., Fisher, J. A., Kim, P. S., Marais, E. A., Zhu, L., Yu, K., Miller, C. C., Yantosca, R. M., Sulprizio, M. P., Thompson, A. M., Wennberg, P. O., Crouse, J. D., St Clair, J. M., Cohen, R. C., Laughner, J. L., Dibb, J. E., Hall, S. R., Ullmann, K., Wolfe, G. M., Pollack, I. B., Peischl, J., Neuman, J. A., and Zhou, X. L.: Why do models overestimate surface ozone in the Southeast United States?, *Atmos. Chem. Phys.*, 16, 13561-13577, doi:10.5194/acp-16-13561-2016, 2016.
- 470 van Geffen, J. H. G. M., Boersma, K. F., Van Roozendaal, M., Hendrick, F., Mahieu, E., De Smedt, I., Sneep, M., and Veefkind, J. P.: Improved spectral fitting of nitrogen dioxide from OMI in the 405-465 nm window, *Atmos. Meas. Tech.*, 8, 1685-1699, doi:10.5194/amt-8-1685-2015, 2015.
- 475 Worden, H. M., Bowman, K. W., Kulawik, S. S., and Aghedo, A. M.: Sensitivity of outgoing longwave radiative flux to the global vertical distribution of ozone characterized by instantaneous radiative kernels from Aura-TES, *J. Geophys. Res.*, 116, doi:10.1029/2010jd015101, 2011.
- Ziemke, J. R., Chandra, S., and Bhartia, P. K.: "Cloud slicing": A new technique to derive upper tropospheric ozone from satellite measurements, *J. Geophys. Res.*, 106, 9853-9867, doi:10.1029/2000jd900768, 2001.